Modeling and Control of a V2G Charging Station Based on Synchronverter Technology

Dongqi Liu, Qingchang Zhong, *Fellow*, *IEEE*, Yaonan Wang, and Guorong Liu

***Abstract*—This paper proposes an idea for modeling and control of a V2G charging station (CS) for electric vehicles (EVs) by using synchronverter technology. First, the architecture of the CS is introduced. Then, a T-S fuzzy controller is designed to decide the reference real power of the synchronverter by considering the grid frequency. Due to the inner frequency- and voltage-drooping mechanisms of the synchronverter, the input and output real and reactive power of the CS will be automatically adjusted on the basis of the reference value according to the degree of deviation from the nominal value of the grid frequency and voltage. To ensure the safety of this operation, an adaptive frequency droop coefficient mechanism is designed to adapt the change of the total energy storage of a CS unit by changing the slope of the P-f control characteristic of the synchronverter. The performance of the CS with the proposed control strategy is investigated with EVs of different battery states, different users' sets and under different grid status. Simulation results demonstrate that the proposed strategy can not only effectively perform controlled charging/discharging of each single electric vehicle inside the CS, but also improve the performance of the electricity grid in terms of efficiency, stability and reliability.**

***Index Terms*—Electric vehicle (EV), synchronverter, smart grid, vehicle-to-grid (V2G), virtual synchronous machines (VSM).**

I. Introduction

ELECTRIC vehicles (EVs) will play a vital role in the future transportation systems since this technology is promising for both energy security and the environment. One vital issue is whether current power grids can sustain the growing demand due to the growing number of EVs and what method should be used to charge these vehicles. To address these concerns, in recent years, many researchers have studied the "V2G" technology [1]–[3], which means EVs serve in both charge and discharge mode and realize bi-directional power flow between cars and power lines. Former studies [1]–[15] have shown that the V2G system is able to provide additional opportunities for grid operators, such as reactive power support [6], active power regulation, load balancing by valley filling and peak load shaving [7], [8], and is able to provide ancillary services such as frequency control and spinning reserves [9]–[12] so that the grid efficiency [13]–[15] is improved. These studies, however, are primarily focused on the power system scheduling with aggregated EVs, which largely depends on the communications between the Independent System Operator (ISO) and the EV aggregators, and lacks the necessary study of low-level control.

Usually, EVs are connected to the power grid through power electronic converters, like all types of renewable energy sources. In general, when the penetration of EVs and renewable sources is relatively low, the stability of the power grid can be controlled by a large synchronous generator which is widely used in conventional thermal power plants or hydro power plants. However, as the trend of EVs and renewable sources' penetration is increasing in future power grids, the large synchronous generator is likely to no longer be able to maintain the stability of the whole power grid. The key problem is, the power electronic converter, which is widely used as the interface for EVs and renewables to plug into the power grid, lacks damping and inertia and does not have the same synchronous characteristics as the synchronous generator does. Hence, when the penetration of EVs and renewables is high, the power grid could lose its robustness due to power fluctuations and failures. To address the problem, researchers have proposed a so-called "virtual synchronous machine (VSM)" [16], [17] method to control the power electronic converter so that it can mimic the dynamic characteristics of a real synchronous machine. A synchronverter [18] is a type of VSM. Its controller has embedded the same mathematical model of a real synchronous machine so that a grid-connected synchronverter can behave like a real grid-connected synchronous machine and is able to realize autonomous frequency and voltage regulation for the grid due to its inner frequency- and voltage- drooping mechanism. Additionally, it is worth mentioning that synchronverter technology is a voltage-controlled strategy, equipped with converters that are able to provide voltage support to the grid when the grid is weak and when conventional current-controlled strategies such as the PQ control strategy are not able to [19].

In this paper, an original control method is proposed to con-

Manuscript received October 13, 2016; revised August 9, 2017; accepted October 9, 2017; date of publication September 30, 2018; date of current version July 30, 2018. This work was supported in part by the National Key Research and Development Program of China (No. 2018YFB0904000 and No. 2018YFB0904003) and National Natural Science Foundation of China (No. 51807013 and No. 51807011).

D. Q. Liu is with the School of Electrical and Information Engineering, Changsha University of Science and Technology, Changsha 410114, China.

Q. C. Zhong (corresponding author, e-mail: zhongqc@ieee.org) is with the Electrical and Computer Engineering Department, Illinois Institute of Technology, Chicago, IL 60616 USA.

Y. N. Wang (co-corresponding author, e-mail: yaonan@hnu.edu.cn) is with the College of Electrical and Information Engineering, Hunan University, Changsha 410082, China.

G. R. Liu is with the School of Computer and Communication, Hunan Institute of Engineering, Xiangtan 411104, China.

DOI: 10.17775/CSEEJPES.2016.01430

trol the bi-directional converters of a V2G supporting charging station (CS) based on the synchronverter technology. The CS is composed of several CS units connected in parallel and using synchronverters as the AC/DC interfaces between each CS unit and the grid. A T-S fuzzy controller is designed to decide the reference set power of the synchronverter, which also translates the real power-frequency (P-f) control characteristics of the synchronverter, by considering the grid frequency (which is estimated by the synchronverter itself) and the battery status of each individual EV inside the unit. An adaptive frequency drooping coefficient mechanism is designed to modify the imaginary mechanical friction coefficient to adapt the change of the energy capacity of the DC bus. A power distribution strategy is proposed to distribute the total real power of a CS unit to every EV inside it and ensure the charging/discharging power of each EV is subject to its limit. By using the proposed method, a CS can be integrated into the power grid and behave in the same way as large synchronous machines do, so that the CS equipped with the proposed control strategy and the power grid can be taken as a whole, hence the power system itself is more robust to disturbance such as frequency fluctuation or failure. This technology has already been demonstrated for over 100 years of operation in the power system demonstrating that the synchronization mechanism of synchronous machines is able to maintain the stability of the power system. Additionally, a synchronverter based V2G charging station adds damping and inertia to the power grid, which could make the operation of the grid smoother [19]. This characteristic is vital when the penetration level of EVs is large. The proposed CS is able to not only realize smart bi-directional charging control of electric vehicles regarding the EVs' SoC and grid status but also provide high-quality frequency and voltage regulation services for the grid due to the inner frequency- and voltage-drooping mechanisms of the synchronverter.

The rest of this paper is organized as follows: Section II introduces the structure and the basic idea of operating the proposed V2G charging station (CS). The synchronverter technology is reviewed in Section III. Section IV proposes a synchronverter-based control strategy for the proposed V2G charging station, where a T-S fuzzy controller [21] is designed to generate the reference set power of the synchronverter, and an adaptive drooping coefficient mechanism is proposed to ensure the safety of the frequency droop operation. Additionally, a power distribution strategy is proposed for control of power flow between different EVs. The performance of the proposed strategy is tested by simulations in the different scenario and the results are discussed in Section V. Finally, conclusions are given in Section VI.

II. Modeling of a V2G Charging Station for Electric Vehicles

The proposed V2G charging station (CS) for electric vehicles is composed of several CS units connected in parallel, where a CS unit consists of three subunits: Control Unit (CU), Synchronverter (SV), and DC Unit. SV functions as a bi-directional converter to combine the grid and the DC unit. Its reference set power and imaginary mechanical friction coefficient is determined by the control unit consisting of four parts: capacity calculation unit, T-S fuzzy control unit, power distribution unit, and adaptive drooping coefficient unit. The DC unit is composed of a DC bus, several EVs connecting to the DC bus, and DC-DC converters. The layout of a CS unit is shown in Fig. 1. The operational process of a proposed CS unit is summarized as follows:

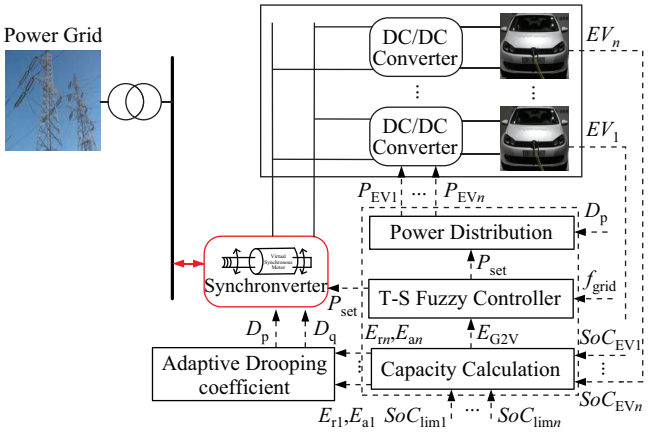

Fig. 1. Conceptual system framework.

1) All the information of EVs' state of charge (SoC_1, SoC_2, …, SoC_n) and constraints ($SoC_{\text{lim}1}$, $SoC_{\text{lim}2}$, …, $SoC_{\text{lim}n}$) are collected and sent to the capacity calculation unit of the CCU ($SoC_{\text{lim}i}$ is the lower SOC limit of EV batteries defined by EV users).

2) The capacity calculation unit of the CCU counts the individual available energy E_{a1}, E_{a2}, …, E_{an} as well as the individual required energy E_{r1}, E_{r2}, …, E_{rn} of each EVs' batteries and then calculates the total available energy E_{V2G} and the total required energy E_{G2V} of the CS unit.

3) Based on the grid frequency f_{grid} which is estimated by the synchronverter itself and the total required energy E_{G2V}, the T-S fuzzy controller calculates the reference set power P_{set} of the CS unit.

4) According to the total available energy E_{V2G}, a proper frequency drooping coefficient of the synchronverter is selected.

5) According to the result of T-S fuzzy controller P_{set} and the selected frequency drooping coefficient of the synchronverter, and according to the individual available energy E_{ai}, the individual required energy E_{ri}, as well as the maximum power limit of each EVs, calculates the reference charging/discharging power P_{EV1}, P_{EV2}, …, P_{EVn} of each EVs t and the final set power P_{set} of the synchonverter simultaneously.

6) According to the calculation results in step 4 and step 5, the synchronverter will be set to realize the autonomous interaction between the CS and the grid.

III. Overview of the Synchronverter Technology

In this paper, synchronverters, which are converters that mimic synchronous machines [18], [19], are introduced as

being the bi-directional DC-AC converter between the DC bus and the grid. The power part of a synchronverter is shown in Fig. 2. The inductance L_s and resistance R_s of the LC filter are the impedance of stator windings of an imaginary synchronous generator (SG), as shown in Fig. 3.

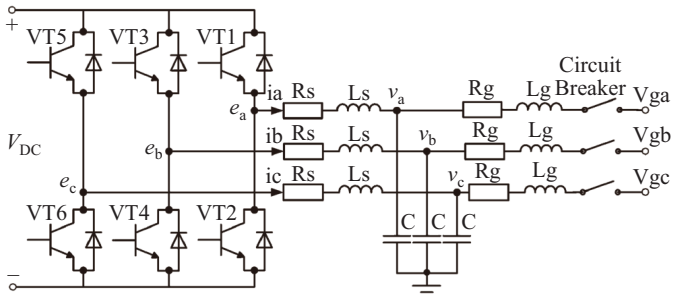

Fig. 2. Power part of a synchronverter.

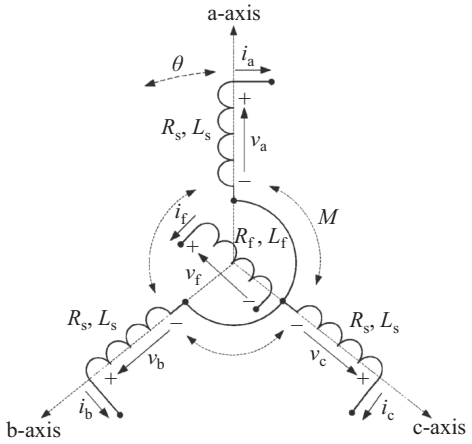

Fig. 3. Structure of an idealized three-phase round-rotor synchronous machine.

The capacitor voltage $[v_a, v_b, v_c]^T$ is the terminal voltage of the SG, and the inductor current $[i_a, i_b, i_c]^T$ is the stator current of the imaginary SG. The mathematical model of the SV can be formulated as shown in Fig. 4, which includes the mathematical model of a three-phase round-rotor synchronous machine described by:

$$\ddot{\theta} = \frac{1}{J}(T_m - T_e - D_p\dot{\theta}) \tag{1}$$

$$T_e = M_f i_f \left\langle i, \widetilde{\sin\theta} \right\rangle \tag{2}$$

$$e = \dot{\theta} M_f i_f \sin\theta \tag{3}$$

$$Q = -\dot{\theta} M_f i_f \left\langle i, \widetilde{\cos\theta} \right\rangle \tag{4}$$

In Fig. 4, T_m is the mechanical torque of the rotor, which is also the control input of the SV; T_e is the electromagnetic torque of the rotor; J is the imaginary moment of the inertia of the rotor; D_p is the imaginary mechanical friction coefficient of the rotor, which is also the drooping coefficient of the frequency droop control loop; i_f is the field excitation current and M_f is the mutual inductance between the stator windings and the field winding; θ is the rotor angle while $\dot{\theta}$ is the virtual angular speed of the machine; i is the stator current flowing out of the machine; Q is the reactive power; e is the back EMF due to the movement of the imaginary rotor; $\widetilde{\sin\theta}$ and $\widetilde{\cos\theta}$ are defined as:

$$\widetilde{\sin\theta} = \begin{bmatrix} \sin\theta \\ \sin(\theta - 2\pi/3) \\ \sin(\theta + 2\pi/3) \end{bmatrix}, \widetilde{\cos\theta} = \begin{bmatrix} \cos\theta \\ \cos(\theta - 2\pi/3) \\ \cos(\theta + 2\pi/3) \end{bmatrix} \tag{5}$$

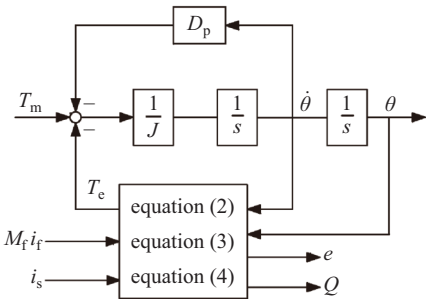

Fig. 4. Mathematical model of a synchronverter.

After mathematical modeling of the SV, the model will be embedded in the DSP controller of a three-phase converter, and the back EMF e is the control signal sent to the PWM generator. According to the area equivalence principle it can be concluded from the reference in Fig. 2. After filtering the output voltage e of the converter through the LC filter, the voltage on the capacitor C can be equivalent to the virtual stator voltage. It can be seen that if the mathematical model and the real synchronous generator are given the same input, i.e. the prime mover mechanical torque, magnetic inductance and excitation current of a synchronous machine, the same output voltage as the stator side of the real synchronous generator can be obtained on the bridge arm of the SV. Since the internal mathematical principles, as well as the external physical representation, are the same as a real synchronous machine, the synchonverter is also called a virtual synchronous machine.

IV. Synchronverter-based Control Strategy for the Proposed V2G Charging Station

In this section, a synchronverter-based control strategy for the V2G charging station is proposed as shown in Fig. 5. The upper part of Fig. 5 is the frequency droop control loop designed for regulating real power, i.e. charging and discharging power of the charging station; the lower part of Fig. 5 is the voltage droop control loop, by which the charging station is able to provide the grid reactive power for voltage support.

In the frequency droop control loop, $\dot{\theta}_n$ is the nominal frequency of the grid, $\dot{\theta}_r$ is the reference frequency of the real power droop control, a PI controller is adopted to regulate the output ΔT of the frequency droop block to be 0 and to generate a small $\Delta\dot{\theta}_r$, $\Delta\dot{\theta}_r$ is then added to the nominal frequency $\dot{\theta}_n$ so that $\dot{\theta}_r$ is generated which is nearly the same as the grid frequency. A detailed demonstration of this self-frequency tracking performance can be found in the literature [20]. Based on this self-frequency tracking performance,

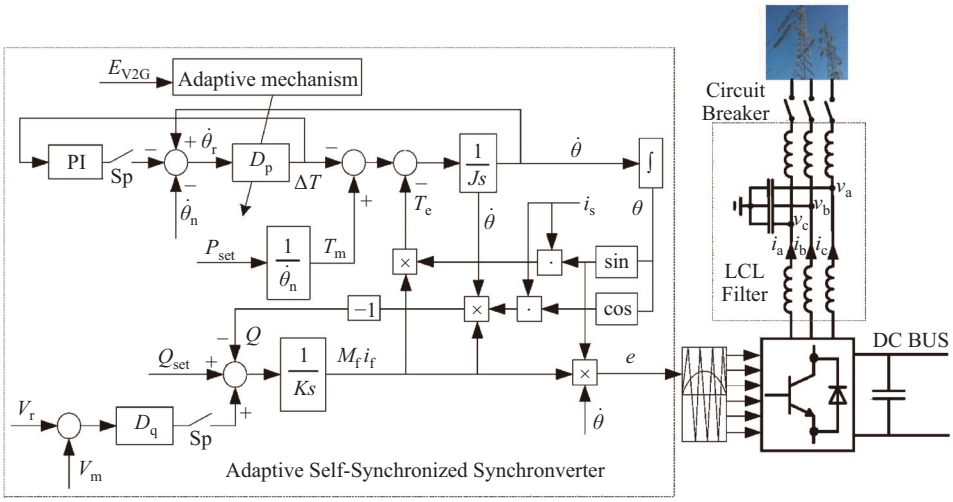

Fig. 5. Control of a synchronverter (SV).

SV does not need a dedicated synchronization unit, such as a phase-locked loop (PLL), to provide phase references. This simplifies the operation of the controller, reduces the cost and prevents control errors caused by the use of PLL. D_p is the drooping coefficient of the frequency droop control, which is defined as:

$$D_p = -\frac{\Delta T}{\Delta\dot{\theta}} \approx \frac{\Delta P}{\Delta\dot{\theta}\cdot\dot{\theta}_n} = \frac{P_n \cdot x\%}{(\dot{\theta}_n)^2 \cdot y\%} \tag{6}$$

where P_n is the rated real power of the synchronverter, $\dot{\theta}_n$ is the nominal grid frequency, and the physical meaning of (6) is a drop of $y\%$ in the grid frequency that can cause the torque (also the real power) to increase by $x\%$.

J is the virtual inertia of the rotor, which is defined by D_p and the time constant of the frequency loop τ_f:

$$J = D_p \tau_f \tag{7}$$

In the voltage droop control loop, V_n is the nominal value of the grid voltage amplitude, V_m is the amplitude of the grid voltage, which is calculated by (assuming the terminal voltage is balanced):

$$V_a V_b + V_b V_c + V_c V_a = -\frac{3}{4} V_m^2 \tag{8}$$

D_q is defined as the ratio of the required change of the reactive power ΔQ to the change of the voltage ΔV:

$$D_q = -\frac{\Delta Q}{\Delta V} = \frac{Q_n \cdot x\%}{V_n \cdot y\%} \tag{9}$$

where Q_n is the rated reactive power of the synchronverter, and the physical meaning of (9) is a drop of $y\%$ of the grid voltage that causes the reactive power to increase by $x\%$.

The error between the reference value Q_{ref} and the reactive power Q is fed into an integrator with a gain $1/K$ to generate $M_f i_f$, where K is defined by D_q, nominal grid frequency $\dot{\theta}_n$ and the time constant of the voltage loop τ_v:

$$K = \dot{\theta}_n D_q \tau_v \tag{10}$$

The real power-frequency (P-f) control characteristic and reactive power-voltage (Q-V) control characteristic of the synchronverter is shown in Fig. 6.

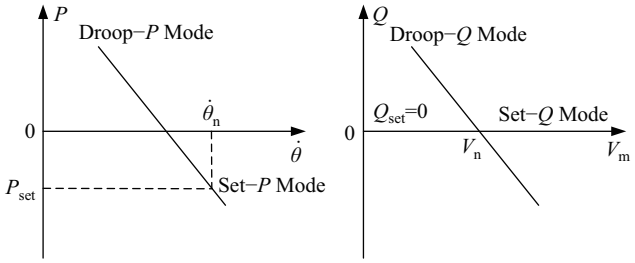

Fig. 6. P-f and Q-V control characteristic of the synchronverter.

It can be seen from Fig. 6, when SV works in the Set-P mode, the output power of SV tracks the reference P_{set}, which means the power output of the virtual prime mover. When the synchronverter works in the Droop-P mode, the output power of SV is a linear function of the grid frequency. The slash shown in Fig. 6 will be translated according to the position of the reference P_{set}. D_p is the slope of the slash. Obviously, a greater D_p means the same frequency change would cause larger real power changes in response. Set-Q mode and Droop-Q mode are similar to the Set-P mode and Droop-P mode, so there is no more tautology here.

Different operational modes of the SV can be selected by turning on or off the switches as shown in Table I. In this paper, when the grid frequency is higher than its nominal value, then the synchronverter is operating in Set-P, Droop-Q mode; when the grid frequency is equal to or lower than its nominal value, and the total available energy of the CS unit is $E_{V2G} > 0$, then the SV is operating in Droop-P, Droop-Q mode.

A. *Decision of* P_{set}

As has been discussed above, the P-f control characteristic of the SV can be translated by a given different reference set power P_{set}, as shown in Fig. 7. The basic idea of translating the

TABLE I
OPERATION MODES OF A SYNCHRONVERTER

Switch Sp	Switch Sq	Mode
ON	ON	Set-P, Droop-Q
ON	OFF	Set-P, Set-Q
OFF	ON	Droop-P, Droop-Q
OFF	OFF	Droop-P, Set-Q

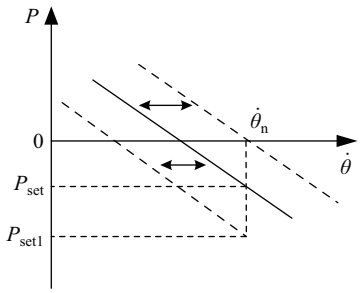

Fig. 7. Different P_{set} translates the P-f control characteristic of the SV.

P-f control characteristic is the concept of secondary frequency control in the power system. The virtual prime mover will raise up its real power output when the grid frequency is dropping and will cut it down when the grid frequency is rising. Considering the particularity of the EV charging station, the reference set power P_{set} should also refer to the battery status of EVs inside the charging station. Hence, a T-S fuzzy controller is adopted here to decide the reference set power, which is also the quantity of the translation of the P-f control characteristic of the SV.

1) Capacity Calculation

According to the EVs' state of charging and constraints, the individual available energy E_{ai}, the individual required energy E_{ri}, as well as the maximum capacity of each EV's batteries $E_{\text{max}i}$ can be calculated by [22]:

$$E_{\text{a}i} = \begin{cases} V_{\text{t}i} Q_i \left(SoC_i - SoC_{\text{lim}i}\right) & E_{\text{a}i} > 0 \\ 0 & E_{\text{a}i} < 0 \end{cases} \tag{11}$$

$$E_{\text{r}i} = \begin{cases} V_{\text{t}i} Q_i \left(100\% - SoC_i\right) & E_{\text{r}i} > 0 \\ 0 & E_{\text{r}i} < 0 \end{cases} \tag{12}$$

$$E_{\text{MAX}i} = V_{\text{t}i} Q_i \tag{13}$$

where V_{ti} and Q_i are the terminal voltage and the rated capacity of the EV_i's battery respectively.

Then the total available energy E_{V2G} and total required energy E_{G2V} of the CS unit can be calculated by:

$$\begin{cases} E_{\text{V2G}} = \sum_{i=1}^{n} E_{\text{a}i} \\ E_{\text{G2V}} = \sum_{i=1}^{n} E_{\text{r}i} \end{cases} \tag{14}$$

2) T-S Fuzzy Control

As mentioned above, a T-S fuzzy controller is designed to generate the reference charging power P_{ref} for the CS unit according to the value of f_{grid} and E_{G2V}. The triangular membership function is used here to define fuzzy variables ($\tilde{f}_{\text{grid}}$ and $\tilde{E}_{\text{G2V}}$) as it is easier to calculate:

$$\mu_{\tilde{A}}(x) = \begin{cases} (x-l)/(m-l) & l < x \le m \\ (r-x)/(r-m) & m < x \le r \\ 0 & \text{otherwise} \end{cases} \tag{15}$$

where l and r are the lower and upper limits of the fuzzy number $\tilde{A}$ and m is the middle value.

The discourse domain of the fuzzy variable $\tilde{f}_{\text{grid}}$ is [0.996, 1.004], which is transferred from f_{grid}'s original domain [49.8, 50.2]. Three fuzzy subsets, i.e. Small (S), Middle (M), and Large (L) have been chosen for $\tilde{f}_{\text{grid}}$ as shown in Fig. 8(a).

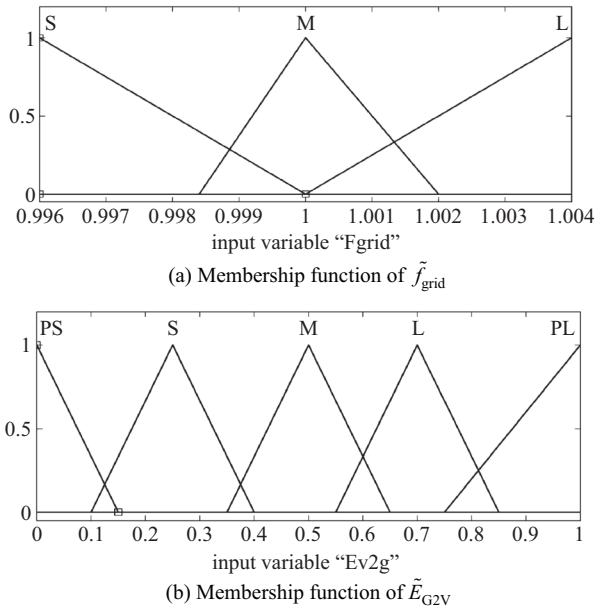

(a) Membership function of $\tilde{f}_{\text{grid}}$

(b) Membership function of $\tilde{E}_{\text{G2V}}$

Fig. 8. Membership function of the two fuzzy sets.

The discourse domain of the fuzzy variable $\tilde{E}_{\text{G2V}}$ is [0,1], which is transferred from E_{G2V}'s original domain [0, E_{MAX}], where E_{MAX} is a variable that is related to the number of EVs integrated in a CS unit:

$$E_{\text{MAX}} = \sum_{i=1}^{n} E_{\text{max}i} \tag{16}$$

Five fuzzy subsets, i.e. Plus Small (PS), Small (S), Middle (M), Large (L), and Plus Large (PL)) have been chosen for $\tilde{E}_{\text{G2V}}$ as shown in Fig. 8(b).

The rule of the FLC is as shown in (17):

$$\begin{aligned} &R_a^i : \text{if } x_1 \text{ is } A_1^i \text{ and } x_2 \text{ is } A_2^i \\ &\text{then } P_{\text{c}}^i = f^i(x_2) \\ &i = 1, 2, \cdots, m \end{aligned} \tag{17}$$

where $x_1 = f_{\text{grid}}$, $x_2 = E_{\text{G2V}}$, $A_1^i \in \tilde{f}_{\text{grid}}$, $A_2^i \in \tilde{E}_{\text{G2V}} p_{\text{c}}^i$ is the charging power of the CS unit determined by rule i, which is designed here as a linear function of E_{G2V}:

$$p_{\text{c}}^i = f^i(x_2) = \frac{\lambda_a^i}{T_0} E_{\text{G2V}} + \lambda_b^i n P_{\text{cm}} \tag{18}$$

where n is the number of EVs in the CS unit, P_{cm} is the nominal charging power of the EVs, T_0 is a time constant, which can be calculated by:

$$T_0 = \frac{MAX(E_{\text{MAX}i})}{P_{\text{cm}}} \tag{19}$$

$\lambda_a^i \in [0,1]$ and $\lambda_b^i \in [0, 0.3, 0.5, 0.8, 1]$ are constants whose values are determined by the value of f_{grid} and E_{G2V}. If the required energy E_{G2V} is very small, then λ_a^i is equal to 1 and λ_b^i is equal to 0 so that p_{c}^i is able to track the change of E_{G2V}, hence the batteries of the EVs will not be overcharged. If E_{G2V} is not very small, λ_a^i is equal to 0 and λ_b^i is equal to 1, the value of p_{c}^i is self-adjusted according to E_{G2V} and f_{grid}. The rule base for selection of λ_a^i and λ_b^i is given in Table II.

TABLE II
RULE BASE FOR FLC

$\tilde{f}_{\text{grid}}$	$\tilde{E}_{\text{G2V}}$	λ_a^i	λ_b^i	$\tilde{f}_{\text{grid}}$	$\tilde{E}_{\text{G2V}}$	λ_a^i	λ_b^i
S	*PS*	1	0	*M*	*L*	0	0.8
S	*S*	0	0.3	*M*	*PL*	0	1
S	*M*	0	0.5	*L*	*PS*	1	0
S	*L*	0	0.5	*L*	*S*	0	0.5
S	*PL*	0	0.8	*L*	*M*	0	0.5
M	*PS*	1	0	*L*	*L*	0	0.8
M	*S*	0	0.3	*L*	*PL*	0	1
M	*M*	0	0.5	/	/	/	/

According to Table II, the output of FLC is formulated as:

$$P_{\text{set}} = \frac{\sum_{i=1}^{15} p_{\text{c}}^i \prod_{l=n}^{2} \mu_{A_n^i}(x_n)}{\sum_{i=1}^{15} \prod_{n=1}^{2} \mu_{A_n^i}(x_n)} = \bar{f}_1(x_1, x_2) E_{\text{G2V}} + \bar{f}_2(x_1, x_2) \tag{20}$$

where $\bar{f}_1(x_1, x_2)$ and $\bar{f}_2(x_1, x_2)$ are non-linear functions:

$$\begin{cases} \bar{f}_1(x_1, x_2) = \dfrac{\sum_{i=1}^{15} \lambda_a^i \prod_{n=1}^{2} \mu_{A_n^i}(x_n)}{\sum_{i=1}^{15} \prod_{n=1}^{2} \mu_{A_n^i}(x_n)} \cdot \dfrac{1}{T_0} \\ \bar{f}_2(x_1, x_2) = \dfrac{\sum_{i=1}^{15} \lambda_b^i \prod_{n=1}^{2} \mu_{A_n^i}(x_n)}{\sum_{i=1}^{15} \prod_{n=1}^{2} \mu_{A_n^i}(x_n)} \cdot nP_{\text{cm}} \end{cases} \tag{21}$$

After obtaining the current grid frequency and EV battery status at each sampling time, the reference charging power of each CS unit can be calculated by (20) and (21).

B. Adaptive Frequency Drooping Coefficient

In this paper, the DC bus of the CS unit connects a number of EVs. Since the number and battery level of these EVs varies widely, it is hard to set a suitable frequency drooping coefficient for an SV in all possible energy storage situations of the DC bus when the SV is operating in Droop-P mode. For example, if the total battery energy level of the EVs connected to the DC bus is low (the number of EVs in the CS is small, or the SoC of the EVs in the CS is low), a large frequency drooping coefficient may cause over discharging of the EV batteries when the grid frequency is much lower than its nominal value. If the total battery energy level of the EVs connected to the DC bus is high, a relatively small frequency drooping coefficient cannot achieve the best performance based on frequency regulation. Hence, when the SV is operating in Droop-P mode, it would be better if the frequency drooping coefficient can be self-adjusted according to the battery level of the EVs connected to the DC bus.

According to the battery SoC limits set by EV users, the total available energy E_{V2G} of a CS unit can be calculated by (4). Assuming E_{m} is the maximum capacity of a CS unit, then the ratio of E_{V2G} to E_{m} can be divided into 5 parts within the closed interval [0,1], as shown in Fig. 9.

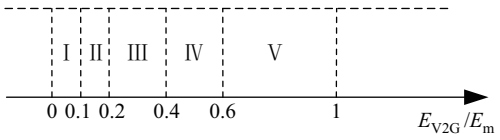

Fig. 9. Battery level of a CS unit.

If $E_{\text{V2G}}/E_{\text{m}}$ is within the range V, which means the available energy for V2G of EVs is very high (and far from SoC lower limits), a large frequency drooping coefficient can be selected to achieve better frequency regulation performance. If $E_{\text{V2G}}/E_{\text{m}}$ is within the range I, which means the number of EVs connected to the CS unit or the total available energy of the EVs is low, a small frequency droop coefficient should be selected to avoid over discharge. Based on the analysis above, assuming the rated power of the SV is 50 kW, then the frequency droop coefficient of the SV can be chosen from Table III, which is calculated by (6) and means a drop of 2.5%, 1.5%, 1%, 0.8%, 0.5% of the grid frequency (from its nominal value) respectively, causing a 100% increase of the real power.

TABLE III
RULE BASE FOR FLC

Zone	I	II	III	IV	V
D_{p}	20.26	33.77	50.66	63.33	101.3

The P-f characteristic of the adaptive drooping coefficient SV is shown in Fig. 10.

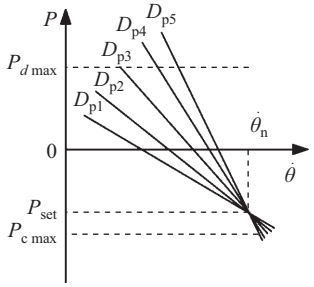

Fig. 10. P-f characteristic of the adaptive drooping coefficient synchronverter.

C. Power Distribution

A power distribution strategy is designed to distribute the input/output power of the SV to each EV that is connected to the DC bus of the CS unit. The charging/discharging power of the EVs can be calculated by:

$$\begin{cases} P_{\mathrm{EV}i} = \dfrac{E_{\mathrm{r}i}}{E_{\mathrm{G2V}}} P_{\mathrm{G2V}} + \dfrac{E_{\mathrm{a}i}}{E_{\mathrm{V2G}}} \left[D_{\mathrm{p}} \dot{\theta}_{\mathrm{n}} (\dot{\theta} - \dot{\theta}_{\mathrm{n}}) \right] & \dot{\theta}_{\mathrm{g}} \le \theta_{\mathrm{n}} \\ P_{\mathrm{EV}i} = \dfrac{E_{\mathrm{r}i}}{E_{\mathrm{G2V}}} P_{\mathrm{G2V}} & \dot{\theta}_{\mathrm{g}} > \theta_{\mathrm{n}} \end{cases} \tag{22}$$

where $P_{\mathrm{EV}i}$ is the reference power of each EV in the charging station. E_{V2G} and E_{G2V} are the total available and required energies of the CS unit; $E_{\mathrm{a}i}$ and $E_{\mathrm{r}i}$ are the available and required energy of each EV. By using the proposed strategy, the charging and discharging power of the EVs are determined by the output of the fuzzy controller, grid frequency, the frequency drooping coefficient, individual EV required or available energy as well as the proportion that is the required or available energy of each individual EV to the whole CS unit.

For safety concerns, in order to prevent the $P_{\mathrm{EV}i}$ exceeding the maximum charging power P_{cm}, or the maximum discharging power P_{dm}, $P_{\mathrm{EV}i}$ is subject to the constraints as:

$$\begin{cases} P_{\mathrm{EV}i} = P_{\mathrm{cm}} & P_{\mathrm{EV}i} \ge P_{\mathrm{cm}} \\ P_{\mathrm{EV}i} = -P_{\mathrm{dm}} & P_{\mathrm{EV}i} < -P_{\mathrm{dm}} \end{cases} \tag{23}$$

Finally, the real power set point of the synchronverter P'_{set} turned out to be:

$$P'_{\mathrm{set}} = \begin{cases} -\sum_{i=1}^{n} P_{\mathrm{EV}i} + D_{\mathrm{p}} \dot{\theta}_{\mathrm{n}} \left(\dot{\theta} - \dot{\theta}_{\mathrm{n}} \right) & \dot{\theta} \le \theta_{\mathrm{n}} \\ -\sum_{i=1}^{n} P_{\mathrm{EV}i} & \dot{\theta} > \theta_{\mathrm{n}} \end{cases} \tag{24}$$

D. DC-DC Converters

The DC bus of the CS is connected with a series of EVs, the topology of the DC-DC converter for EVs is shown in Fig. 11, which is a bi-directional half-bridge buck-boost converter. If there is only one EV connected to the DC bus, the controller of the DC-DC converter is shown in Fig. 12, where the outer loop is to control the DC bus voltage and the inner loop is to control the inductor current, and the charging/discharging power of the EV flows automatically. If the number of EVs connected to the DC bus is more than one, then the controller for the rest of the EVs is as shown in Fig. 13, where $P_{\mathrm{EV}i}$ is divided by the EV battery voltage(V_t) to obtain the reference current(I_{ref}) and then a PI controller is applied to control the current flow in or out of the batteries [22].

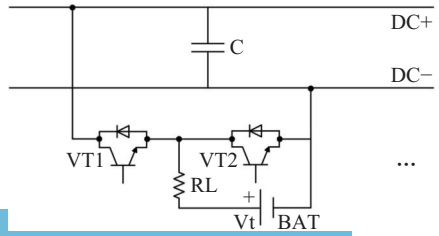

Fig. 11. Topology of DC-DC converter.

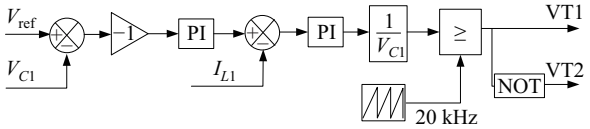

Fig. 12. DC-DC converter controller 1.

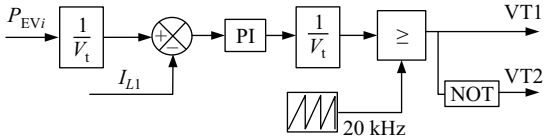

Fig. 13. DC-DC converter controller 2.

V. Simulation Results and Discussion

Simulations were carried out in the environment of a MATLAB∼R2015a/SIMULINK/Simscape/SimPowerSystem. The solver used in the simulation was an ode23tb with a relative tolerance of 10^{-3} and a maximum step size of 0.2 ms. The parameters of the circuit used in the simulations are given in Table IV. The LCL filter design method is referred to in [23]. Three cases are considered for testing the effectiveness of the proposed CS with its sychronverter based control strategy:

TABLE IV
Parameters of the Simulation Circuit

Parameters	Values	Parameters	Values
L_{s}	150 μH	L_{g}	450 μH
R_{s}	0.045 Ω	R_{g}	0.135 Ω
C	22 μF	R	1000 Ω
L_{vr}	1 mH	R_{vr}	0.1 Ω
C_{dc}	10 mF	L_{dc}	20 mH
R_{dc}	0.1 Ω	K_{p}	0.02
K_i	0.4	DC bus voltage	700 V
Grid rated frequency	50 Hz	Nominal voltage (line-line)	380 V

Case 1: EVs' batteries with a different initial SOC connected during normal hours (assuming grid frequency is 1.0 p.u. at the beginning and will then drop to 0.999 p.u. at t = 10 s, and grid voltage is 1.0 p.u.);

Case 2: EVs' batteries with a different initial SOC connected during peak hours (assuming grid frequency is 0.996 p.u. at the beginning and will then raise up to 0.997 p.u. at t = 10 s, and grid voltage is 0.98 p.u.);

Case 3: EVs' batteries with a different initial SOC connected during valley hours (assuming grid frequency is 1.004 p.u. at the beginning and will then drop to 1.003 p.u. at t = 10 s, and grid voltage is 1.02 p.u.).

Simulations were performed considering a V2G charging station including 3 CS units with 12 EVs in it; EV_1–EV_5 are with unit 1, EV_6–EV_{10} are with unit 2, and EV_{11}–EV_{12} are with unit 3. The different initial state of charges (SoC) and user defined SOC limits of each EV are given in Table V. The rated

TABLE V
BATTERIES SPECIFICATION IN DIFFERENT SCENARIOS

i	SoC_{lim}	Initial SoC		
		Case 1	Case 2	Case 3
EV_1	10%	50%	50%	50%
EV_2	10%	60%	60%	60%
EV_3	10%	70%	70%	70%
EV_4	10%	80%	80%	80%
EV_5	10%	95%	95%	95%
EV_6	10%	30%	30%	30%
EV_7	10%	40%	40%	40%
EV_8	10%	50%	50%	50%
EV_9	10%	80%	80%	80%
EV_{10}	10%	90%	90%	90%
EV_{11}	10%	60%	60%	60%
EV_{12}	10%	80%	80%	80%

capacity of each EV battery is 100 Ah, the rated battery voltage of each EV is 300 V. The power part of the charging station includes 3 parallel-operated SVs with 3 DC units connected to it. Assume the maximum charging and discharging power of each EV is $P_{\rm cm} = 10$ kW, $P_{\rm dm} = -10$ kW; the rated real power of each synchronverter is 50 kW, the rated reactive power of each SV is 10 kVar; the voltage drooping factor $D_{\rm q}$ was chosen as 644.6, which means a voltage droop of 5% will cause the reactive power to increase by 100%. The time factor of the droop loops were chosen as $\tau_{\rm f} = 0.002$ s and $\tau_{\rm v} = 0.002$ s.

A. Case Study

1) Case 1: EVs Connected During Normal Hours

The period when the power grid is neither in peak hour or in valley hour is called the normal hour. Assuming the grid frequency is 1.0 p.u., grid voltage is 1.0 p.u., simulation results of the SV internal frequency, real power, and reactive power of the three CS units as well as battery current of EV_1–EV_{12} are listed as shown in Fig. 14. From Fig. 14(a), it can be seen that the three SVs were quickly synchronized with the grid before the circuit breakers were turned on at $t = 0.5$ s. There was a tiny current surge on the circuit when the grid connect operation was applied at $t = 0.5$ s. Then, at $t = 1$ s, the SVs quickly responded to the real power step change $P_{\rm set}$ which is calculated by (19); since $\dot{\theta} = \dot{\theta}_n$, the value of $P_{\rm set}$ is primarily determined by the output of the T-S fuzzy controller according to the battery level of EVs in the charging station. It can be seen that, when EVs connected during normal hours, CS unit 1 to CS unit 3 are all controlled to charge from the grid. As there are only 2 EVs in CS unit 3, the charging power of unit 3 is relatively lower than that of unit 1 and unit 2. Then, at $t = 10$ s,the grid frequency drops to 0.999 p.u.; it can be seen that the inner frequency of the SV tracks the grid frequency quickly, and the three CS units respond to the change of the grid frequency quickly by cutting down their charging power due to the frequency droop mechanism of the SV. As for the reactive power, as the grid voltage is equal to its nominal value, most of the time the reactive power of the three SVs is the same as the $Q_{\rm set}$ which was always set as 0, but at $t = 0.5$ s, and $t = 1$ s, Q faced a little fluctuation due to the coupling between the real and reactive power. From Fig. 14(b), it can

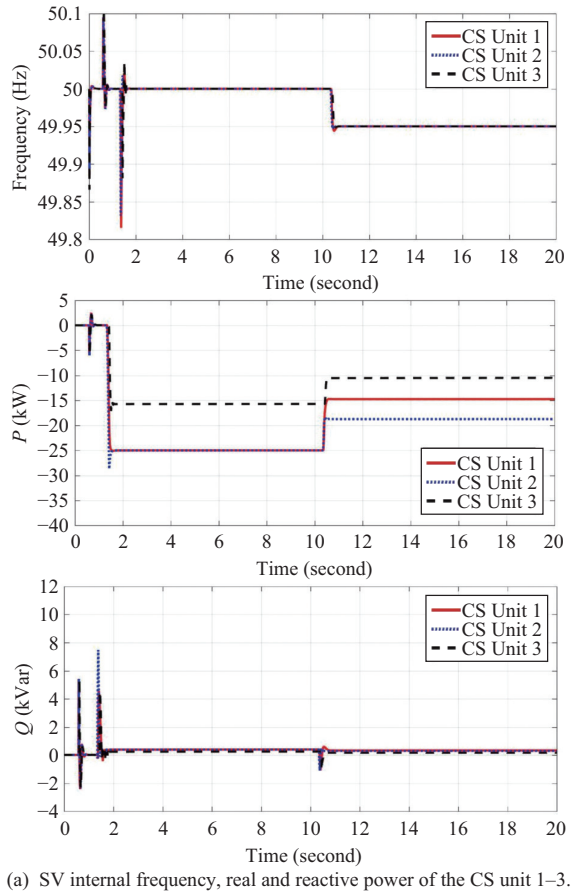

(a) SV internal frequency, real and reactive power of the CS unit 1–3.

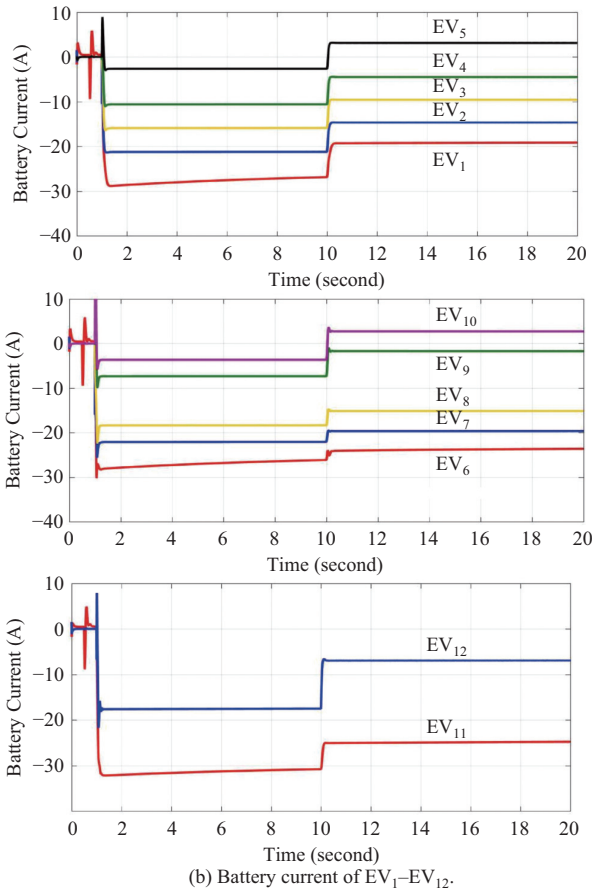

(b) Battery current of EV_1–EV_{12}.

Fig. 14. Simulation results of case 1.

be seen that the battery current of the EVs in each CS unit is changing according to the real power change of the CS unit. The EVs share of the real power of the CS units according to their own battery status. As the user soc limits are set the same, the EV with the lower battery SoC will gain more charging power, hence the battery charging current is higher according to the proposed power distribution strategy such as EV_1–EV_3, EV_6–EV_8, EV_{11}, while the battery charging current of the EVs with a high battery SoC is relatively low such as EV_4–EV_5, EV_9–EV_{10}, and EV_{12}.

2) Case 2: EVs Connected During Peak Hours

When EVs are connected during peak hours, simulation results of SV internal frequency, real power, reactive power of the three CS units as well as battery current of EV_1–EV_{12} are listed as shown in Fig. 15. From Fig. 15(a), it can be seen that the internal frequencies of the three SVs are quickly synchronized with the grid frequency, because the grid frequency is lower than its nominal value, the three SV are operating in Droop-P, Droop-Q mode, the frequency drooping coefficient D_{p} will be selected adoptively according to the battery status of the EVs connected to the DC buses of the SVs. It can be seen that, at $t = 1$ s, CS unit 1 and CS unit 3 are controlled to discharge energy to the grid, while unit 2 is controlled to charge from the grid. The value of the charging/discharging power of the three CS units are determined both by the T-S fuzzy controller and the frequency drooping mechanism of the SVs. As the battery level of the CS unit 1 is relatively high, then a relatively high D_{p} is applied. According to the P-f characteristics of the SV, when $\dot{\theta}-\dot{\theta}_{\mathrm{n}} < 0$, the CS unit will reduce the charging power or discharge to the grid (depend on the value of P_{set}). In this case, since the battery level of CS unit 1 is relatively high, then the basic charging power of CS unit 1 determined by the T-S fuzzy controller is relatively low. Due to a 0.4% deviation of the grid frequency, CS unit 1 discharges energy to the grid. The energy stored in CS unit 2 is lower than unit 1, so it is still charging from the grid. However, when compared with case 1, it can be seen that the charging power of CS unit 2 is greatly reduced, which is also due to the P-f control characteristics of the SV. There are only 2 EVs in CS unit 3, hence a relatively low D_{p} is applied. So the discharging power of CS unit 3 is lower than that of unit 1. Then, at $t = 10$ s, the grid frequency rises up to 0.997 p.u., the inner frequency of the SV tracks the grid frequency quickly, and the three CS units respond quickly to the change of the grid frequency by cutting down their discharging power, raising up their charging power due to the frequency droop mechanism of the SVs. As for reactive power, as the grid voltage is 2% lower than its nominal value, the reactive power of each SV rises up about 4 kVar at $t = 1$ s. From Fig. 15(b), it can be seen that the battery current of the EVs in each CS unit is changing according to the real power change of the CS unit. As the user soc limits are set the same, the EV with a lower battery SoC has a positive battery charging current, which means they are charging energy from the DC bus such as EV_1, EV_6–EV_8; while the battery charging current of the EVs with high battery SoC is discharging such as EV_2–EV_5, EV_9–EV_{10}.

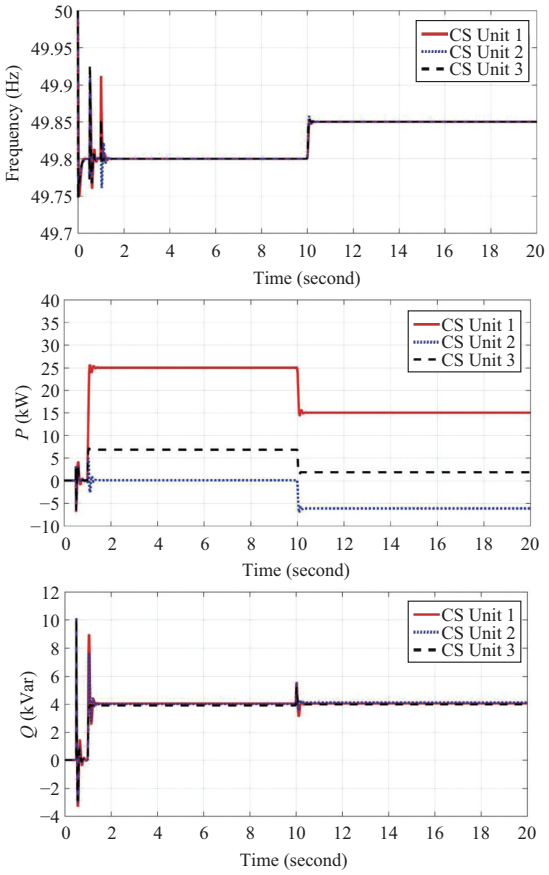

(a) SV internal frequency, real and reactive power of the CS units 1–3.

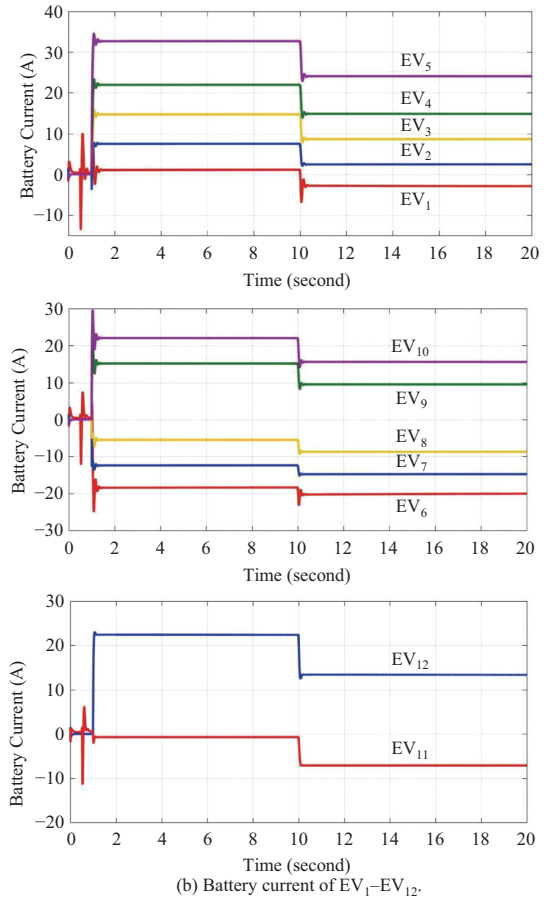

(b) Battery current of EV_1–EV_{12}.

Fig. 15. Simulation results of case 2.

3) Case 3: EVs Connected During Valley Hours

The valley hours of the grid are primarily at midnight. When EVs are connected during valley hours, simulation results of the SV internal frequency, real power, reactive power of the three CS units as well as battery current of EV_1–EV_{12} are listed, as shown in Fig. 16. Because the grid frequency is higher than its nominal value, the three SVs of the CS units are operating in Set-P, Droop-Q mode. From Fig. 16(a), it can be seen that, at $t = 1$ s, all three CS units are controlled to absorb energy from the grid with different charging power. The value of real power is determined by T-S fuzzy controllers according to the energy requirement of each of the EVs inside the unit. It can be seen that the battery level of CS unit 1 is higher than unit 2, hence the charging power of unit 1 is lower than unit 2. Unit 3 only contains 2 EVs, hence its charging power is the lowest among the three units. At $t = 10$ s, the grid frequency drops to 1.003 p.u, which is still higher than its nominal value, the three SVs of the CS units are operating in P_{set} mode; to avoid overcharge, the real power of the three CS units are kept the same value as P_{set}. As for reactive power, as the grid voltage is 2% higher than its nominal value, the reactive power of each SV dropped by about 4 kVar at $t = 1$ s. From Fig. 16(b), it can be seen that, as the user soc limits are set the same, the EV with a lower battery SoC is charging with higher power such as EV_1–EV_2, EV_6–EV_8, EV_{11}; while the battery charging current of the EVs with high battery SoC is charging with a lower power such as EV_4–EV_5, EV_9–EV_{10}, EV_{12}.

From the simulations above, it can be seen that although the initial SoC and users' limits of the EVs are the same among the three cases, the real power of the CS during peak hours, valley hours, and normal hours are quite different. The simulation results have shown the regulation ability of the CS to control the charging/discharging power of the EVs in different grid scenarios.

Fig. 17 shows the changing of energy stored in the three CS units in cases 1–3, where E_{G2V} is the total energy requirement of the CS unit and E_{V2G} is the total available energy of the CS unit. It can be seen in Fig. 17 that in case 1 and case 3, while the grid frequency is the nominal value or higher than the nominal value, E_{G2V} of the three CS units is dropping and E_{V2G} is rising, which means the total energy level of the three CS units is increasing. In case 2, while the grid frequency is lower than the nominal value, E_{G2V} of CS unit 1 and CS unit 3 is rising and that of CS unit 2 is dropping, the trend of E_{V2G} is just the opposite, which means the total energy level of CS unit 1 and CS unit 3 is decreasing, and that of CS unit 2 is increasing. The change of energy stored in the three CS units in cases 1–3 are consistent with the real power change of the three CS units, as shown in Fig. 14–Fig. 16.

B. Long-term Simulation

A long-term simulation has been carried out by considering a proposed V2G charging station include 6 CS units with 30 EVs plugged into the grid at $t = 0$ h. Assuming that the 24-hour grid frequency is shown as Fig. 18. Assuming the SoC and the users' set of all the EVs in the charging station

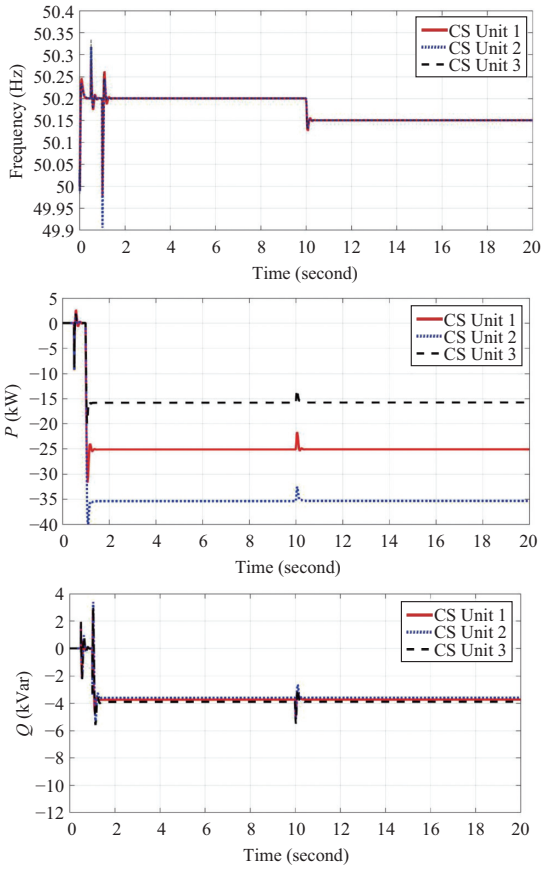

(a) SV internal frequency, real and reactive power of the CS units 1–3.

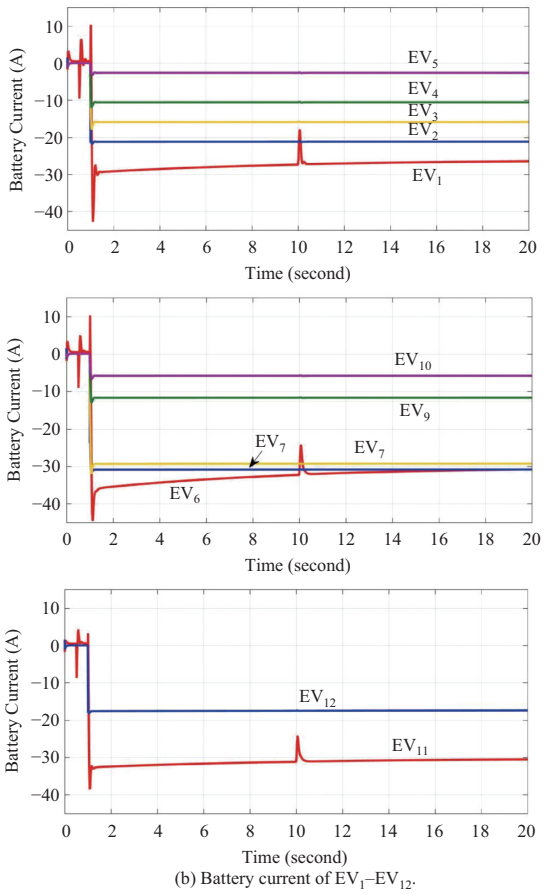

(b) Battery current of EV_1–EV_{12}.

Fig. 16. Simulation results of case 3.

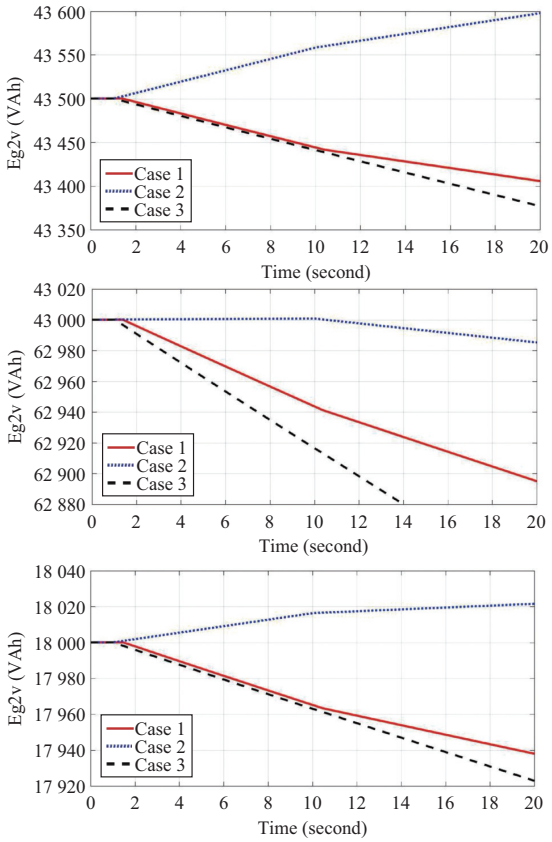

(a) E_{G2V} in three cases of the CS unit 1, unit 2, unit 3 respectively from top to bottom.

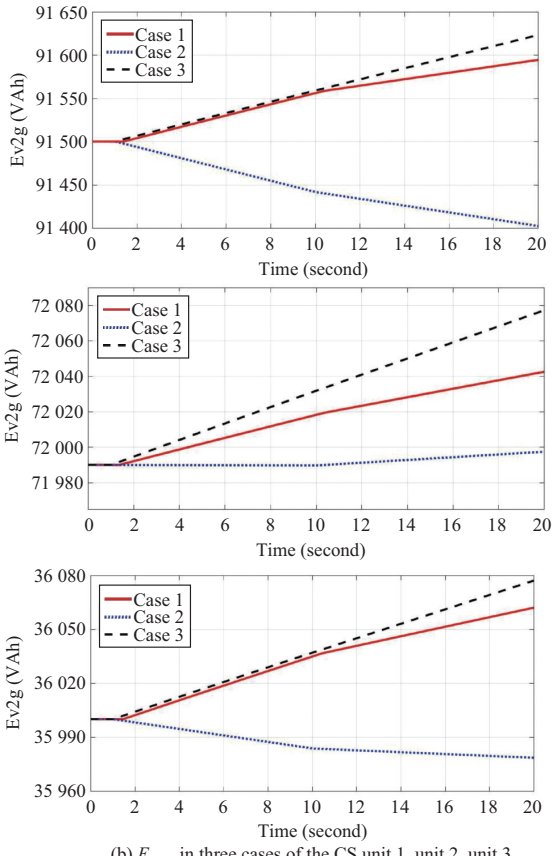

(b) E_{V2G} in three cases of the CS unit 1, unit 2, unit 3 respectively from top to bottom.

Fig. 17. Energy stored of the three CS units in case 1–3.

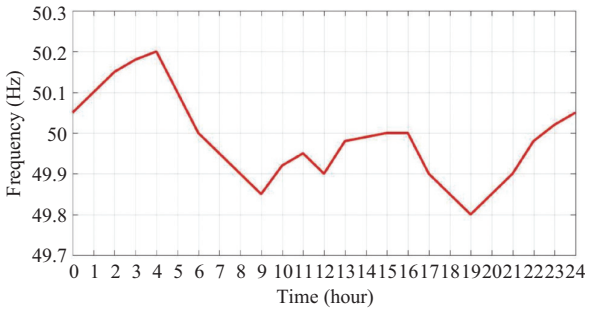

Fig. 18. 24-hour grid frequency.

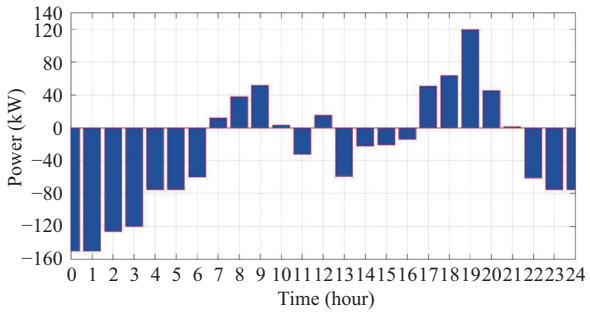

Fig. 19. 24-hour CS power output.

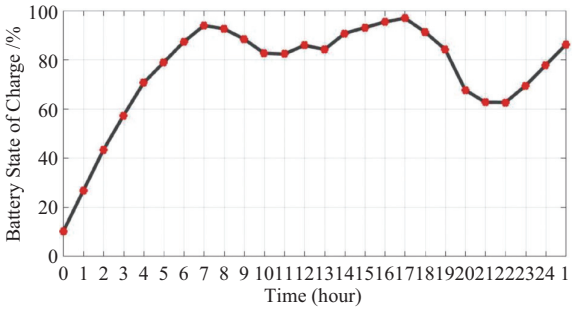

Fig. 20. 24-hour EV battery SoC curve.

TABLE VI
FREQUENCY DROOPING COEFFICIENT

EV(i)	Q_{ti}	V_{ti}	SoC_{limi}	SoC_i
EV_1–EV_{30}	200 Ah	300 V	10%	10%

are the same as Table VI. The output power of the proposed V2G charging station in 24 hours is shown in Fig. 19, and the change of battery SoC in 25 hours is shown in Fig. 20.

From Fig. 19 and Fig. 20 it can be seen that when the grid is in valley hours, i.e. 0:00–6:00, the grid frequency is high, the CS is controlled to absorb excess energy from the grid; the battery SoC of the EVs is gradually rising up when the grid is in peak hours, i.e. 7:00–21:00, and the CS is controlled to feed energy back to the grid. It is worth mentioning that the value of the charging or discharging power of the CS is not only related to the grid frequency but also related to the battery state of charge of the EVs inside the CS. For example, the grid frequency at 4:00 is higher than that at 3:00, but the

charging power of the CS at 4:00 is lower than that at 3:00. This is due to the fact that the EVs' battery level at 4:00 is relatively high after a 4-hour high power charge. As the energy required is reduced, the charging power is also reduced. It also can be seen that the grid frequencies are the same at 9:00 and at 18:00, which is lower than the nominal grid frequency. But the battery level of the EVs at 18:00 is higher than that of 9:00, thus the output power of the former is higher. At 19:00, due to a sharp decrease in grid frequency, the discharging power of the CS jumped rapidly, while at 20:00, due to the EVs having discharged a lot of energy to the grid, their battery SoCs were reduced so that their discharging power was reduced as well. It can be seen from the long-term simulation that, the proposed V2G charging station is able to regulate its input/output power according to the battery status of the EVs inside the CS in different grid scenarios, and it is also able to provide frequency regulation service to the grid while meeting the energy demand of the EV users.

Assuming that the base load of the very grid that the CS is plugged in is described in the red line, as shown in Fig. 21, according to Fig. 18, the load with the proposed V2G charging station can be calculated as shown by the blue line. Obviously, after employing the proposed V2G charging station, the peak load of the grid is cut down significantly, and the valley load is increased greatly. The result of this simulation demonstrates that the proposed methodology is able to play a key role in peak shaving and valley filling for the power network, thus promoting the efficiency of the electricity grid.

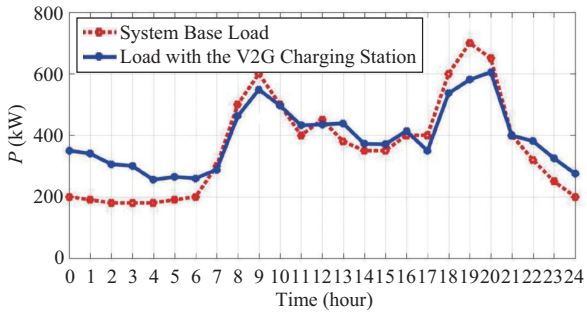

Fig. 21. 24-hour system load with and without the V2G charging station.

VI. Conclusion

This work proposed a control method for V2G charging stations based on the synchronverter technology. The CS is composed of several CS units connected in parallel and using synchronverters as the AC/DC interfaces between each CS unit and the grid. The main features of the proposed method can be summarized as follows.

1) A T-S fuzzy controller is designed to decide the reference charging power of the CS unit according to the grid frequency, which is estimated by the synchronverter itself, and the charging demand of each individual EV inside the unit.

2) When the synchronverter works in Droop-P mode ($\dot{\theta} < \dot{\theta}_n, E_{V2G} > 0$), the output power of the CS unit is determined by the frequency droop control characteristics of the synchronveter, which means a drop in the grid frequency would cause a decrease of the reference charging power (or an increase of discharging power) of the CS unit in response.

3) An adaptive frequency drooping coefficient mechanism is designed to modify the frequency drooping coefficient (also the slope of the P-f control characteristics) of the synchronverter to adapt the change of the energy capacity of the DC bus.

4) By using the proposed method, a CS can be integrated into the power grid and behave in the same way as large synchronous machines do, so that the CS equipped with the proposed control strategy and the power grid can be taken as a whole based on the well-known synchronous mechanism. The proposed CS also adds damping and inertia to the power grid, which makes the operation of the grid smoother.

Simulation results have verified that the proposed strategy can not only effectively perform controlled charging/discharging of each single EV inside the CS, but also provide high-quality frequency and voltage regulation services for the grid as well.

References

[1] S. Habib, M. Kamran, and U. Rashid, "Impact analysis of vehicle-to-grid technology and charging strategies of electric vehicles on distribution networks," *Journal of Power Sources*, vol. 277, pp. 205–214, Mar. 2015.

[2] P. D. Lund, J. Lindgren, J. Mikkola and J. Salpakari, "Review of energy system flexibility measures to enable high levels of variable renewable electricity," *Renewable & Sustainable Energy Reviews*, vol. 45, pp. 785–807, May 2015.

[3] E. L. Karfopoulos, and N. D. Hatziargyriou, "Distributed Coordination of Electric Vehicles providing V2G Regulation Services," *IEEE Transactions on Power Systems*, vol. 31, no. 1, pp. 2834–2846, Jan. 2016.

[4] M. Yilmaz, and P. T. Krein, "Review of impact of vehicle-to-grid technologies on distribution systems and utility interface," *IEEE Transactions on Power Electronics*, vol. 28, no. 12, pp. 5673–5689, Dec. 2013.

[5] K. F. Abdollah, T. Niknam, and M. Fotuhi-Firuzabad, "Stochastic reconfiguration and optimal coordination of V2G plug-in electric vehicles considering correlated wind power generation," *IEEE Transactions on Sustainable Energy*, vol. 6, no. 3, pp. 822–830, Jul. 2015.

[6] M. C. Kisacikoglu, B. Ozpineci, and L. M. Tolbert, "EV/PHEV Bidirectional Charger Assessment for V2G Reactive Power Operation," *IEEE Transactions on Power Electronics,* vol. 28, no. 12, pp. 5717–5727, Dec. 2013.

[7] L. Zhang et al., "Coordinating plug-in electric vehicle charging with electric grid: Valley filling and target load following," *Journal of Power Sources*, vol. 267, no. 1, pp. 584–597, Dec. 2014.

[8] N. Chen, C. W. Tan, and T. Q. S. Quek, "Electric Vehicle Charging in Smart Grid: Optimality and Valley-Filling Algorithms," *IEEE Journal of Selected Topics in Signal Processing*, vol. 8, no. 6, pp. 1073–1083, Dec. 2014.

[9] S. Siyamak et al., "Potential of vehicle-to-grid ancillary services considering the uncertainties in plug-in electric vehicle availability and service/localization limitations in distribution grids," *Applied Energy*, vol. 171, no. 1, pp. 523–540, Jun. 2016.

[10] E. Sortomme, and M. A. El-Sharkwi, "Optimal scheduling of vehicle-to-grid energy and ancillary services," *IEEE Transactions on Smart Grid*, vol. 3, no. 1, pp. 351–359, Mar. 2012.

[11] Sekyung Han, Soohee Han, and Kaoru Sezaki, "Development of an optimal vehicle-to-grid aggregator for frequency regulation," *IEEE Transactions on Smart Grid*, vol. 1, no. 1, pp. 65–72, Jun. 2010.

[12] H. Liu et al., "Decentralized vehicle-to-grid control for primary frequency regulation considering charging demands," *IEEE Transactions on Power Systems*, vol. 28, no. 3, pp. 3480–3489, Aug. 2013.

[13] N. Mehdi et al, "Light-duty electric vehicles to improve the integrity of the electricity grid through vehicle-to-grid technology: Analysis of regional net revenue and emissions savings," *Applied Energy*, vol. 168, pp. 146–158, Apr. 2016.

[14] A. K. Srivastava, B. Annabathina, and S. Kamalasadan, "The challenges and policy options for integrating plug-in hybrid electric vehicle into the electric grid," *The Electricity Journal*, vol. 23, no. 3, pp. 83–91, Apr. 2010.
[15] Z. Li, Q. Guo, H. Sun et al., "Emission-concerned wind-EV coordination on the transmission grid side with network constraints: Concept and case study," *IEEE Transactions on Smart Grid*, vol. 4, no. 3, pp. 1692–1704, sep. 2013.
[16] Q. C. Zhong, "Virtual Synchronous Machines: A unified interface for grid integration," *IEEE Power Electronics Magazine*, vol. 3, no. 4, pp. 18–27, Dec. 2016.
[17] Q. C. Zhong, *Power electronics-enabled autonomous power systems: next generation smart grids*, NJ: Wiley-IEEE Press, 2017.
[18] Q. C. Zhong, and G. Weiss, "Synchronverters: Inverters that mimic synchronous generators. Industrial Electronics," *IEEE Transactions on Industrial Electronics*, vol. 58, no. 4, pp. 1259–1267, Apr. 2011.
[19] Q. C. Zhong, P. L. Nguyen, Z. Ma, and W. Sheng, "Self-synchronized synchronverters: inverters without a dedicated synchronization unit," *IEEE Transactions on Power Electronics*, vol. 29, no. 2, pp. 617–630, Feb. 2014.
[20] Q. C. Zhong, and D. Boroyevich, "Structural resemblance between droop controllers and phase-locked loops," *IEEE Access,* vol. 4, no. 99, pp. 5733–5741, Sep. 2016.
[21] T. Takagi, and M. Sugeno, "Fuzzy identification of systems and its applications to modeling and control," *IEEE Transactions on Systems, Man, and Cybernetics*, vol. SMC-15, no.1, pp. 116–132, Feb. 1985.
[22] T. Kannan et al., "Modeling and control of contactless based smart charging station in V2G scenario," *IEEE Transactions on Smart Grid*, vol. 5, no. 1, pp. 337–348, Jan. 2014.
[23] H. Kamalesh et al., "Active damping of output LC filter resonance for vector-controlled VSI-Fed AC motor drives," *IEEE Transactions on Industrial Electronics*, vol. 59, no. 1, pp.334–342, Jan. 2012.

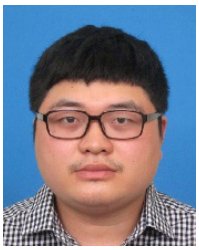

Dongqi Liu received his B.S. degree in electronic information engineering from the University of Shanghai for Science and Technology, Shanghai, China, in 2008, and his Ph.D. degree in control science and engineering (awarded the Outstanding Graduates Prize) from Hunan University, Changsha, China, in 2017. He worked for Shanghai Electric Group Co. as an Engineer from 2008 to 2010. He worked in the Department of Electrical and Computer Engineering, Illinois Institute of Technology, Chicago as a visiting researcher from 2015 to 2016 under the sponsorship of the Chinese Scholarship Council. Since 2017, he has been a Lecturer in the School of Electrical and Information Engineering, Changsha University of Science and Technology. His research interests include electric vehicles, renewable energy, smart grid integration, etc.

Qingchang Zhong (F'17) received his Ph.D. degree in control and power engineering (awarded the Best Doctoral Thesis Prize) from Imperial College London, London, U.K., in 2004 and his Ph.D. degree in control theory and engineering from Shanghai Jiao Tong University, Shanghai, China, in 2000. He is the Max McGraw Endowed Chair Professor in Energy and Power Engineering at the Department of Electrical and Computer Engineering, Illinois Institute of Technology, Chicago, USA, and the Research Professor in Control of Power Systems at the Department of Automatic Control and Systems Engineering, The University of Sheffield, UK. He is a Distinguished Lecturer of both the IEEE Power Electronics Society and the IEEE Control Systems Society. His research focuses on power electronics, advanced control theory and the integration of both, together with applications in renewable energy, smart grid integration, electric drives and electric vehicles, aircraft power systems, high-speed trains, etc.

Yaonan Wang received his B.S. degree in computer engineering from East China Technology Institute, Fuzhou, China, in 1981, and his M.S. and Ph.D. degrees in control engineering from Hunan University, Changsha, China, in 1990 and 1994, respectively. Since 1995, he has been a Professor with the College of Electrical and Information Engineering, Hunan University. His research interests include hybrid electric vehicle control, intelligent control theory and its applications.

Guorong Liu received his B.S. degree and M.S. degrees in industrial automation from Hunan University, Changsha, China, in 1981 and 1986, respectively, and his Ph.D. degree in control engineering from Xi'an Jiaotong University, Xi'an, China, in 2003. Since 1997, he has been a Professor with Hunan Institute of Engineering, Xiangtan, China. His research interests include intelligent control theory and applications and modern AC motor control.